The University of
Nottingham

UNITED KINGDOM · CHINA · MALAYSIA

Greig, Bradley and Bolton, James S. and Wyithe, J.
Stuart B. (2015) The impact of temperature fluctuations
on the large-scale clustering of the Lyα forest. Monthly
Notices of the Royal Astronomical Society, 447 (3). pp.
2503-2511. ISSN 1365-2966

Access from the University of Nottingham repository:
http://eprints.nottingham.ac.uk/42510/1/stu2624.pdf

The impact of temperature fluctuations on the large-scale clustering of the Lyα forest

Bradley Greig,[1,2,3]★ James S. Bolton[3,4] and J. Stuart B. Wyithe[2,3]

[1]*Scuola Normale Superiore, Piazza dei Cavalieri 7, I-56126 Pisa, Italy*
[2]*School of Physics, University of Melbourne, Parkville, VIC 3010, Australia*
[3]*ARC Centre of Excellence for All-sky Astrophysics (CAASTRO) 44-70 Rosehill Street, Redfern NSW 2016, Sydney, Australia*
[4]*School of Physics and Astronomy, University of Nottingham, University Park, Nottingham NG7 2RD, UK*

ABSTRACT

We develop a semi-analytic method for assessing the impact of the large-scale IGM temperature fluctuations expected following He II reionization on three-dimensional clustering measurements of the Lyα forest. Our methodology builds upon the existing large volume, mock Lyα forest survey simulations presented by Greig et al. by including a prescription for a spatially inhomogeneous ionizing background, temperature fluctuations induced by patchy He II photoheating and the clustering of quasars. This approach enables us to achieve a dynamic range within our semi-analytic model substantially larger than currently feasible with computationally expensive, fully numerical simulations. The results agree well with existing numerical simulations, with large-scale temperature fluctuations introducing a scale-dependent increase in the spherically averaged 3D Lyα forest power spectrum of up to 20–30 per cent at wavenumbers $k \sim 0.02\,\mathrm{Mpc}^{-1}$. Although these large-scale thermal fluctuations will not substantially impact upon the recovery of the baryon acoustic oscillation scale from existing and forthcoming dark energy spectroscopic surveys, any complete forward modelling of the broad-band term in the Lyα correlation function will none the less require their inclusion.

Key words: intergalactic medium – quasars: absorption lines – cosmology: theory – large-scale structure of Universe.

1 INTRODUCTION

The Lyα forest is a powerful probe of large-scale structure in the intergalactic medium (IGM). It is characterized by a series of narrow absorption features imprinted into the spectra of bright background sources, and arises from the resonant scattering of Lyα photons by intervening neutral hydrogen (Rauch 1998). The observed transmitted flux yields information on the underlying physical properties of the IGM, such as the gas density, ionization state and temperature, and is sensitive to the matter power spectrum at small scales, 1–$80\,h^{-1}\,\mathrm{Mpc}$, along the line of sight (Croft et al. 2002; Viel, Haehnelt & Springel 2004; McDonald et al. 2006; Seljak, Slosar & McDonald 2006; Palanque-Delabrouille et al. 2013).

Recently, Busca et al. (2013, see also Slosar et al. 2013; Delubac et al. 2014; Font-Ribera et al. 2014) reported the first successful detection of baryon acoustic oscillations (BAOs) in the Lyα forest from the Baryon Oscillation Spectroscopic Survey (BOSS). These observations have highlighted the potential of the Lyα forest for probing the *three-dimensional* large-scale clustering of structure

within the IGM, in addition to the existing 1D line-of-sight measurements. However, these data (as well as results from forthcoming surveys such as eBOSS and DESI) will also be sensitive to large-scale fluctuations of *astrophysical* origin. Large-scale variations in the ionization and thermal state of the IGM in particular may be detectable at $2 < z < 3$ (Slosar et al. 2009; White et al. 2010; McQuinn et al. 2011). Indeed, both Pontzen (2014) and Gontcho A Gontcho, Miralda-Escudé & Busca (2014) have recently developed analytical models for investigating the impact of very large scale ($k < 0.01\,h\,\mathrm{Mpc}^{-1}$) ionization fluctuations on the Lyα forest. At the mean BOSS redshift of $z \sim 2.3$, these studies concluded there should be a measurable impact on the H I power spectrum at large scales as a result of the interplay between the clustering of the IGM and fluctuations in the underlying H I fraction.

However, significant fluctuations in the IGM temperature of the order of $\sim 10^4\,\mathrm{K}$ are also expected to linger following the reionization of singly ionized helium (He II) at $z \sim 3$ (McQuinn et al. 2009; Compostella, Cantalupo & Porciani 2013). These will result in large-scale variations in the H I fraction through the temperature dependence of the H II recombination coefficient, $\alpha_{\mathrm{H II}} \propto T^{-0.7}$. Gontcho A Gontcho et al. (2014) briefly discussed the impact that these temperature fluctuations might have on the Lyα power

spectrum, although as noted by these authors, their analytic model was not suitable for fully modelling both the local and global effects of heating during He II reionization. Earlier work by McQuinn et al. (2011) also investigated the signature of temperature fluctuations in the IGM using an analytical argument combined with radiative transfer (RT) simulations of He II reionization (McQuinn et al. 2009). These authors found order of unity variations in the amplitude of the 3D Lyα forest power spectrum at $k < 0.1\,\mathrm{Mpc}^{-1}$. However, the simulations used to perform the McQuinn et al. (2011) analysis were not large enough to sample fluctuations on scales $\lesssim 0.05\,\mathrm{Mpc}^{-1}$, nor were the Lyα forest spectra extracted from the RT simulations able to resolve the Jeans scale at mean density. Self-consistently modelling the expected signature of temperature fluctuations in Lyα spectroscopic surveys is thus extremely computationally challenging. A large dynamic range is required to simultaneously resolve small-scale structure in the Lyα forest and probe sufficiently large cosmic volumes which incorporate the sparse ionizing sources (quasars; e.g. Furlanetto & Oh 2008a) thought to drive the temperature fluctuations.

An alternative approach is therefore to use simplified but significantly more efficient techniques to investigate this problem. In this context, Greig, Bolton & Wyithe (2011, hereafter GBW11) developed an efficient, large-volume mock Lyα forest survey model which was used to simulate the signature of BAOs in the Lyα forest. The results agreed well with a variety of observational measurements after calibration against hydrodynamical simulations, and were additionally able to sample large cosmological volumes ($\sim 1\,\mathrm{Gpc}^3$) at high resolution (~ 240 kpc). In this work, we now extend this model to examine the effect of temperature fluctuations following He II reionization on measurements of large-scale clustering with the Lyα forest.

The paper is organized as follows. In Section 2, we outline modifications made to our previous simulations and then describe our model for large-scale temperature fluctuations in Section 3. We then investigate the impact of these large-scale thermal fluctuations on the Lyα forest in Section 4. Finally, in Section 5, we summarize our results and provide our closing remarks. Throughout this work we assume a Λcolddarkmatter cosmology with, $h = 0.72$, $\Omega_\mathrm{m} = 0.26$, $\Omega_\Lambda = 0.74$, $\Omega_\mathrm{b} = 0.0444$, $n_\mathrm{s} = 0.96$ and $\sigma_8 = 0.8$. These are equivalent to our calibration hydrodynamical simulation, model L3 of Bolton et al. (2010).

2 LARGE-SCALE LYα FOREST SIMULATIONS

Hydrodynamical simulations of the IGM have been enormously successful at reproducing the basic observational properties of the Lyα forest (e.g. Croft et al. 1998; Theuns et al. 1998). However, these simulations are often limited to relatively small volumes ($< 40\,\mathrm{Mpc}^3$) to ensure the spatial resolution is sufficient for fully resolving the Jeans scale in the low-density IGM. Even state-of-the-art IGM simulations (e.g. Lukić et al. 2015) still do not approach the very large (Gpc) scales required to study BAOs in the Lyα forest. In the last few years, this has led to renewed interest in the development of simplified techniques for modelling large-scale correlations in the Lyα forest. These approaches achieve the required dynamic range, but often at the expense of accuracy on small scales where the density field is mildly non-linear. For example, Font-Ribera, McDonald & Miralda-Escudé (2012a) generate Lyα forest spectra by inexpensively generating one dimensional Gaussian fields and subsequently introducing three dimensional correlations into the mock data. Le Goff et al. (2011) generate three dimensional Gaussian density fields and use a lognormal mapping to obtain the IGM density

field. Most recently, Peirani et al. (2014) utilized large-scale dark matter simulations and used conditional probability distributions to directly relate the Lyα transmission to the dark matter density. This latter method is more computationally demanding than the other approaches (although still less so than hydrodynamical simulations), but it has the advantage of capturing small-scale correlations more accurately.

The Lyα forest models in this work are based on the fast, large volume simulations developed by GBW11. This is itself based on a model developed by Viel et al. (2002), whereby a linear density field undergoes a rank-ordered mapping of its probability distribution to the corresponding distribution from a calibration hydrodynamical simulation. In this regard, our approach is most similar to that used by Le Goff et al. (2011). Although this model does not correctly capture the mildly non-linear structure probed by the Lyα forest on small scales, it is very well suited for studying the fluctuations on large scales considered here. We direct the reader to GBW11 for further discussion and tests of our Lyα forest model. Here, we restrict ourselves to describing only the new components we have implemented for examining the effect of temperature fluctuations on Lyα forest clustering following He II reionization. Note that all quantitative results in this work are obtained at redshift $z = 2.5$ using $1\,\mathrm{Gpc}^3$ comoving simulation volumes with 4096^3 pixels.

2.1 Clustering of ionizing sources

Quasars, with their hard non-thermal spectra, are the sources considered most likely to drive the process of He II reionization (Madau, Haardt & Rees 1999; Furlanetto & Oh 2008a; McQuinn et al. 2009). These sources are known to cluster on scales of a few tens of Mpc (Shen et al. 2007) and to be strongly biased tracers of the large-scale structure. Therefore, to develop a physically motivated model for temperature fluctuations in the IGM following He II reionization, we must first identify the location of the quasars in our simulation volume.

We achieve this by performing an iterative procedure to identify suitable locations for the ionizing sources. This begins with a large ($1\,\mathrm{Gpc}^3$) volume box which contains a gridded 4096^3 linear IGM density field in Fourier space. This is then smoothed on a mass-scale of $5 \times 10^{12}\,\mathrm{M_\odot}$ by a top-hat filter in real space, roughly corresponding to the expected characteristic halo mass hosting a luminous quasar. After Fourier transforming the density field to real space, a pixel is then flagged as a candidate quasar location when (i) its smoothed linear density exceeds four times the linear critical density for collapse and (ii) it is the highest density peak within a grid centred on the candidate pixel which extends 8 pixels from centre to edge. Finally, we sort all candidate quasar locations by their smoothed linear overdensity, sampling from highest to lowest. As a test of this procedure, we have computed the quasar correlation function recovered by this approach and verified there is excellent agreement to the observed clustering of luminous quasars presented by Shen et al. (2007).

2.2 Spatial fluctuations in the ionizing background

With our prescription for identifying the locations of the ionizing sources in hand, we now turn to modelling the spatial fluctuations in the ionizing background. We use the method outlined by Bolton & Viel (2011) for this purpose (see also Furlanetto 2009).

First, we must assign luminosities to the quasar locations identified in our simulation volume using the observed quasar luminosity function (QLF). The number of quasars to be placed within our

simulation volume, V, is obtained by integrating the B-band QLF, $\phi(L_B, z)$ of Hopkins, Richards & Hernquist (2007),

$$N(L_B > L_{\min}) = V \int_{L_{\min}}^{\infty} \phi(L_B, z)\, dL_B, \qquad (1)$$

where we assume a limiting magnitude of $L_{\min} = 10^{44.25}$ erg s^{-1} ($M_B = -22$) in this work.

We next assign each quasar a B-band luminosity by Monte Carlo sampling the observed QLF, selecting from our sorted list of candidate quasars until we obtain $N(L_B > L_{\min})$ sources. We assume a broken power-law spectral energy distribution (Madau et al. 1999),

$$L_\nu = \begin{cases} \nu^{-0.3} & (2500 < \lambda < 4600\ \text{Å}), \\ \nu^{-0.8} & (1050 < \lambda < 2500\ \text{Å}), \\ \nu^{-\alpha_s} & (\lambda < 1050\ \text{Å}), \end{cases} \qquad (2)$$

where α_s is the extreme UV index. Telfer et al. (2002) obtained $\alpha_s = 1.57 \pm 0.17$ from a sample of low-redshift, radio-quiet quasars and additionally observed significant source-to-source variations, characterized as a Gaussian distribution with a mean $\alpha_s \approx 1.6$ and a standard deviation of 0.86. More recently, Shull, Stevans & Danforth (2012) and Stevans et al. (2014) recovered a mean spectral index of $\alpha_s = 1.41$ from *HST*-COS observations at $z < 1.5$. We therefore encompass the large observed variability in α_s by Monte Carlo sampling a Gaussian with a mean of 1.5 and standard deviation 0.5 over the range of three standard deviations.

We next calculate $J(\boldsymbol{x}, \nu)$ [erg s^{-1} cm^{-2} Hz^{-1} sr^{-1}], the specific intensity of the ionizing background. For the N quasars in our simulation volume, at frequencies between the H I and He II photoionization edges, $\nu_{\text{H I}} < \nu < \nu_{\text{He II}}$, the total contribution to the ionizing background is given by,

$$J(\boldsymbol{x}, \nu) = \frac{1}{4\pi} \sum_{i=1}^{N} \frac{L_i(\boldsymbol{x}_i, \nu)}{4\pi |\boldsymbol{x} - \boldsymbol{x}_i|^2}, \qquad (3)$$

where $|\boldsymbol{x} - \boldsymbol{x}_i|$ is the distance at a point $\boldsymbol{x}$ to quasar i. We have assumed the IGM is optically thin below the He II ionization threshold; recently reported values for the mean free path for H I ionizing photons at $z = 2.4$ are in the range $\sim$500–860 comoving Mpc (O'Meara et al. 2013; Rudie et al. 2013), which is an appreciable fraction of our 1 Gpc^3 simulation volume. As a result, our simulations do not capture the very large scale ($k < 0.01$ Mpc^{-1}) ionization fluctuations discussed recently by Pontzen (2014) and Gontcho A Gontcho et al. (2014).

At frequencies above the He II ionization threshold, $\nu > \nu_{\text{He II}}$, the ionizing background is instead,

$$J(\boldsymbol{x}, \nu) = \frac{1}{4\pi} \sum_{i=1}^{N} \frac{L_i(\boldsymbol{x}_i, \nu)}{4\pi |\boldsymbol{x} - \boldsymbol{x}_i|^2} e^{-\frac{|\boldsymbol{x} - \boldsymbol{x}_i|}{\lambda_{\text{He II}}} \left(\frac{\nu}{\nu_{\text{He II}}} \right)^{-3(\beta-1)}}, \qquad (4)$$

where $\lambda_{\text{He II}}$ is the mean free path of ionizing photons at the He II ionization threshold, which is a highly uncertain quantity that will vary substantially during He II reionization. Models derived from the observed H I column density distribution report values in the range $\sim$90–114 Mpc at $z = 2.5$ to $\sim$15–36 Mpc (comoving) at $z = 3$ (Khaire & Srianand 2013; Davies & Furlanetto 2014). In this work, we assume $\lambda_{\text{He II}} = 45$ comoving Mpc, which is similar to the expected mean separation of luminous quasars at $z \sim 2.5$ (Davies & Furlanetto 2014). This choice maximises the impact of temperature fluctuations on our results at $z = 2.5$; larger mean free paths will result in smaller temperature fluctuations in our model. Note, however, that since the adiabatic cooling time-scale in the low-density IGM is long, $t \sim H^{-1}$, thermal fluctuations imprinted during He II

reionization at $z \sim 3$ – when the mean free path may be rather short – will also persist to lower redshift, and so the assumption of a smaller mean free path is likely reasonable (see also Gontcho A Gontcho et al. 2014). We further approximate the column density distribution for He II absorbers in the diffuse IGM to follow a power law with $\beta = 1.5$. While this will broadly capture the effect of Poisson distributed absorbers on the frequency dependence of the mean free path, the distribution will start to deviate from a single power law when H I and He II become optically thick (Fardal, Giroux & Shull 1998; Haardt & Madau 2012).

Finally, to calculate the specific intensity, we evaluate equations (3) and (4) using 30 frequency bins spanning the range 1–100 Ryd. The photoionization rates [s^{-1}] are then

$$\Gamma_i(\boldsymbol{x}) = \int_{\nu_i}^{\infty} 4\pi \sigma_i(\nu) J(\boldsymbol{x}, \nu) \frac{d\nu}{h_p \nu}, \qquad (5)$$

and the photoheating rates [erg s^{-1}] are

$$g_i(\boldsymbol{x}) = \int_{\nu_i}^{\infty} 4\pi \sigma_i(\nu) h_p(\nu - \nu_i) J(\boldsymbol{x}, \nu) \frac{d\nu}{h_p \nu}. \qquad (6)$$

Here, the subscript i denotes three species of hydrogen and helium (H I, He I and He II), h_p is the Planck constant, $\sigma_i(\nu)$ is the photoionization cross-section and ν_i is the ionization threshold.

Assuming neutral hydrogen is in photoionization equilibrium, the H I number density at any location within our simulation volume is then obtained via,

$$n_{\text{H I}}(\boldsymbol{x}, z) = \frac{\alpha_{\text{H II}}(T)}{\Gamma_{\text{H I}}(\boldsymbol{x})} \frac{2 - Y}{2(1 - Y)} n_H^2(\boldsymbol{x}, z). \qquad (7)$$

Here, $\alpha_{\text{H II}}(T)$ is the temperature dependent recombination rate, $\Gamma_{\text{H I}}(\boldsymbol{x})$ is the spatially varying photoionization rate determined from equation (5) and Y is the helium mass fraction, for which we assume $Y = 0.24$ (Planck Collaboration XVI 2014).

2.3 Patchy heating from He II reionization

For the final part of our semi-analytical patchy heating model, we use the above calculation of the inhomogeneous ionizing background at $E > 4$ Ryd to estimate the temperature of the IGM following He II reionization (see also Raskutti et al. 2012; Lidz & Malloy 2014 for related approximate approaches for heating during H I reionization at $z > 5$).

During He II reionization, the excess energy of an He II ionizing photon above the ionization threshold goes into heating the IGM, resulting in a substantial boost to the overall temperature. The precise amount of heating will depend on the intrinsic spectral shape of the ionizing background and the degree of hardening as the radiation is filtered through the IGM. In practice, the excess energy per photoionization for a power-law spectrum, $L_\nu \propto \nu^{-\alpha_s}$, will vary between the optically thin and thick limits, $\langle E \rangle_{\text{thin}} = h_p \nu_{\text{He II}}/(\alpha_s + 2)$ to $\langle E \rangle_{\text{thick}} = h_p \nu_{\text{He II}}/(\alpha_s - 1)$ (Abel & Haehnelt 1999).

We may thus estimate the expected temperature boost in the IGM following He II reionization as (Furlanetto & Oh 2008b)

$$\Delta T(\boldsymbol{x}) = 0.035 f_{\text{He II}} \left(\frac{2}{3k_B} \right) \langle E_{\text{He II}}(\boldsymbol{x}) \rangle. \qquad (8)$$

Here, $\langle E_{\text{He II}}(\boldsymbol{x}) \rangle = g_{\text{He II}}(\boldsymbol{x})/\Gamma_{\text{He II}}(\boldsymbol{x})$ is the average excess energy per He II photoionization (which will vary between $\langle E_{\text{thin}} \rangle \sim 15.5$ eV and $\langle E_{\text{thick}} \rangle \sim 108.8$ eV for $\alpha_s = 1.5$) at position $\boldsymbol{x}$ within our simulation volume and $f_{\text{He II}}$ is the He II fraction in the IGM when He II photoheating commences (we assume $f_{\text{He II}} = 1$). This expression assumes the excess energy per He II photoionization is

shared with the baryons in the IGM via Coulomb interactions. Secondary ionizations by fast electrons will only occur ∼1 per cent of the time and can be ignored here (Shull & van Steenberg 1985; McQuinn et al. 2009).

The last step is to then add the temperature boost from equation (8) to an initial thermal state prior to He II reionization. We follow the procedure used in GBW11 and assume the IGM temperature follows a well-defined power-law temperature–density relation at 1 + δ ≤ 10 (e.g. Hui & Gnedin 1997), and a constant temperature at higher overdensites where radiative cooling becomes important, such that

$$T_{init} = T_0 \begin{cases} (1 + \delta_b)^{\gamma - 1} & (1 + \delta_b) \leq 10 \\ 10^{\gamma - 1} & (1 + \delta_b) > 10. \end{cases} \quad (9)$$

In this work, we assume $T_0 = 10\,000$ K, consistent with measurements of the IGM thermal state at $z \sim 4$–5, prior to the onset of He II reionization (Schaye et al. 2000; Lidz et al. 2010; Becker et al. 2011). Note, however, γ is still poorly constrained at these redshifts; we therefore adopt a value of $\gamma = 1.3$ which lies in the middle of the theoretically expected range of $\gamma = 1.0$–1.6.

The IGM temperature in our patchy heating model is then computed by adding the expected temperature boost from He II

photoheating to equation (9),

$$T_{IGM} = T_{init} + \Delta T(\mathbf{x}). \quad (10)$$

As we shall now demonstrate in the next section, this simple, semi-analytical model allows us to qualitatively capture the effect of large-scale temperature fluctuations on the Lyα forest without resorting to expensive RT simulations.

3 THERMAL FLUCTUATIONS IN THE IGM FOLLOWING HE II REIONIZATION

3.1 Predicted heating following He II reionization

Fig. 1 displays the results of our simple model for temperature fluctuations in 250 Mpc^2 slices within our simulation volume. Clockwise from top left, the panels show the rank-ordered non-linear IGM density (see GBW11 for details), the IGM temperature following the addition of a temperature boost from He II photoheating, the H I photoionization rate and the magnitude of the temperature boost predicted by equation (8).

The first point to note is that the quasars – which reside at the positions where $\Gamma_{H\,I}$ is largest in the lower-right panel – clearly trace the overdense regions observed in the upper-left panel, as
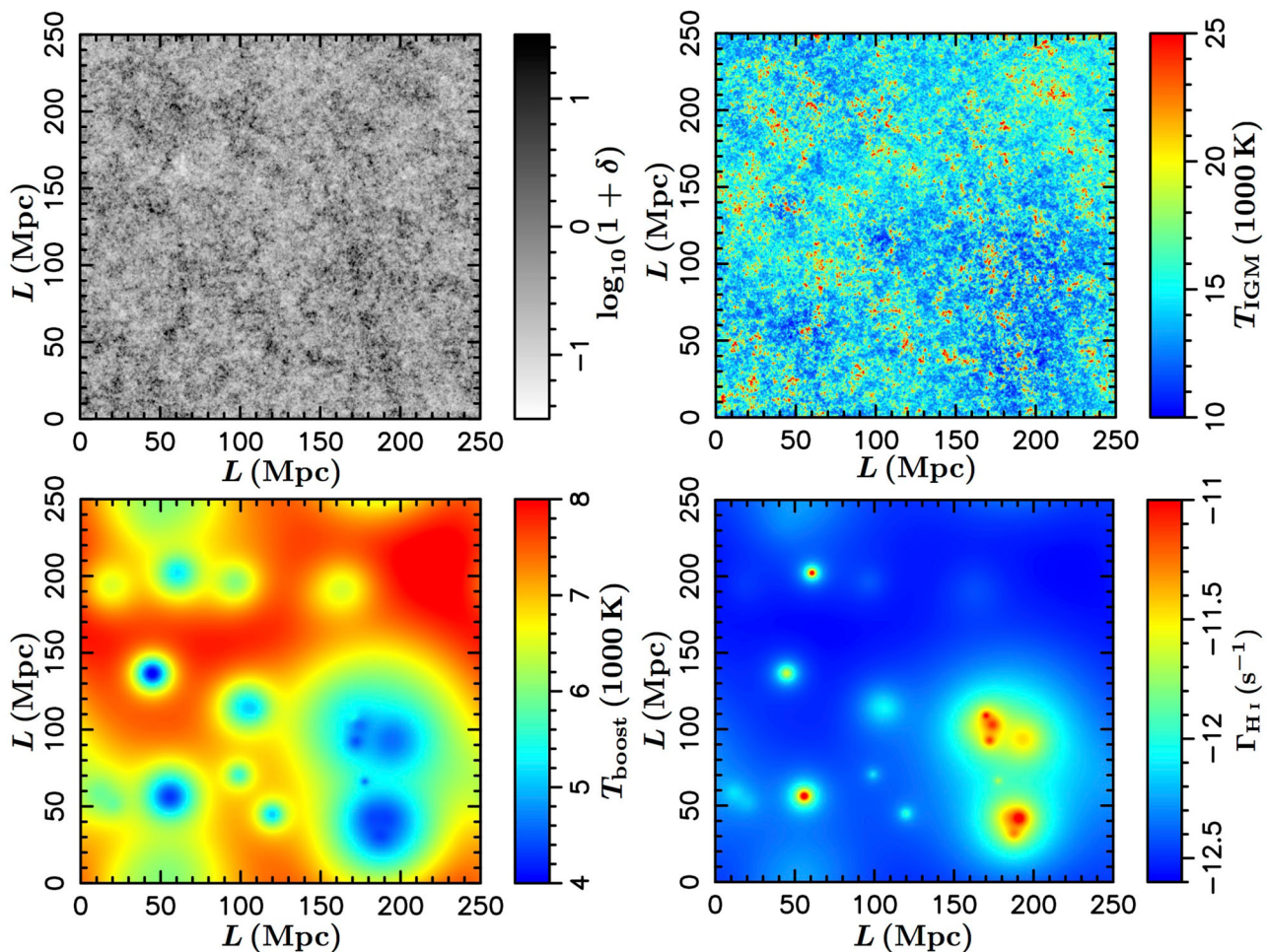

Figure 1. Slices through our Lyα forest model at $z = 2.5$. The slice thickness corresponds to a width of ∼240 kpc (i.e. our simulation resolution). Top left: the rank-ordered IGM density contrast (see GBW11 for details). Top right: the IGM temperature following He II photoheating. Bottom left: the boost to the IGM temperature following He II photoheating. Bottom right: the H I photoionization rate. The clustering of the ionizing sources (quasars) is clearly apparent in this panel.

expected. It is also evident that patchy He II photoheating modifies the IGM temperature substantially, with fluctuations of the order of $\sim 10^4$ K on scales of several hundred Mpc. Regions in the direct vicinity of the quasars are cooler, primarily because they are preferentially heated by softer He II ionizing photons with relatively short mean free paths. Conversely, the furthest regions from the quasars are hottest as they are preferentially ionized by high-energy (hard) ionizing photons with long mean free paths. Qualitatively, this picture is similar to the RT simulations of McQuinn et al. (2009) and Compostella et al. (2013), who also find regions furthest from the quasars tend to be hottest following He II reionization. Note, however, that in the RT simulations, the timing of He II reionization also plays a role – regions close to quasars are ionized first and have a longer time to cool adiabatically. This effect acts in addition to the spectral filtering effect, and is not incorporated into the simple time-independent implementation used here.

Quantitatively, we observe an average temperature boost of ≈ 4000 K in the vicinity of the quasars. Regions of the IGM furthest from the quasars instead typically achieve $\Delta T \approx 8000$–$10\,000$ K. For comparison, McQuinn et al. (2009) find an average temperature boost at mean density of $\approx 12\,000$ K, although some of the regions reionized last in their simulations experience $\Delta T \gtrsim 30\,000$ K. More recent simulations from Compostella et al. (2013) find a slightly lower temperature boost at mean density of $\approx 10\,000$ K. Observational measurements of the IGM temperature from the curvature of the transmitted flux in the Lyα forest also indicate a boost in the IGM temperature of ≈ 8000–$10\,000$ K (for an assumed $\gamma = 1.3$; Becker et al. 2011). Our simple model thus broadly reproduces the expected level of heating in the IGM following He II reionization for gas at mean density. Note, however, we do not recover the $\Delta T \gtrsim 30\,000$ K heating observed in the IGM in the simulations by McQuinn et al. (2009), which is in part due to the fact we have no sub-grid prescription for the (uncertain) additional filtering of the ionizing radiation by dense structures in the IGM (see e.g. Meiksin & Tittley 2012). On the other hand, as the volume filling factor of these very hot regions remains low, and the largest temperature boosts are confined to dense regions $(1 + \delta > 10)$ which are not well probed by the Lyα forest at $z \sim 2.5$, this is unlikely to impact significantly on our results.

3.2 The temperature–density relation

RT simulations of He II reionization also indicate that soon after the commencement of He II reionization, the IGM temperature–density relation may take on a bimodal distribution (Bolton, Oh & Furlanetto 2009; McQuinn et al. 2009; Meiksin & Tittley 2012; Compostella et al. 2013). The recently photoheated gas will tend to follow a separate temperature–density relation to the remainder of the IGM which is yet to be reionized. Following the completion of He II reionization, the bimodal IGM temperature–density relation disappears and the gas starts to cool adiabatically. However, significant scatter (in excess of that expected from optically thin models) and a shallower slope for the temperature–density relation persist.

In Fig. 2, we provide an example IGM temperature–density scatter plot to demonstrate our simple model also captures this effect following He II reionization. The results of our simulation (contours and shaded region) are compared to the assumed power-law expression adopted by GBW11 (red line). The boost in the IGM temperature and the increased scatter in the relationship following He II reionization is clear on comparison to our initial temperature–density relation, T_{init} (blue line). There is furthermore very good agreement between the temperature–density relation in our semi-
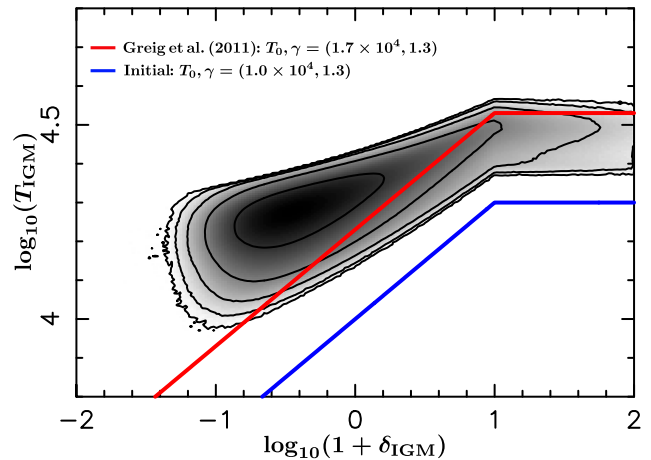

Figure 2. Contour plot of the temperature–density relation recovered from our Lyα forest model at $z = 2.5$. The shaded region corresponds to the normalized frequency of the data while the solid contours represent 90, 70, 50, 30 and 10 per cent of this maximal value. The blue curve corresponds to T_{init}, while the red curve corresponds to the temperature–density relation (without inhomogeneous He II photoheating) used by GBW11.

analytical model and the results from the RT simulations of McQuinn et al. (2009) and Compostella et al. (2013). We find, at all IGM densities, a comparable level of scatter in the IGM temperature and similar (i.e. shallower) slope for the temperature–density relation relative to the value of $\gamma = 1.3$ assumed prior to He II photoheating. Overall, these results give us confidence that our simple model will capture the impact of He II photoheating on the IGM adequately.

4 THE LARGE-SCALE CLUSTERING OF THE LYα FOREST

In the previous sections, we have outlined our semi-analytical prescription for incorporating large-scale temperature fluctuations into the fast, efficient Lyα forest simulations developed by GBW11. We now shift our focus to investigating the impact these fluctuations may have on the Lyα forest, paying particular attention to their effect on the 3D Lyα forest power spectrum.

In what follows, we consider two separate cases. First, a model with the He II photoheating rates implemented as described above, and secondly an otherwise identical model with the added IGM temperature fluctuations using equation (10) removed. In the latter case, we assume a single IGM temperature–density relation, with $T_0 = 17\,000$ K and $\gamma = 1.3$. In each case, we produce 10 independent realizations, enabling us to explore the box-to-box scatter in our models (i.e. cosmic variance). The method for producing Lyα forest spectra from our simulations remains unchanged from GBW11. In summary, we draw synthetic skewers of the IGM density, velocity and temperature fields from our semi-analytic model and compute the total transmitted flux, $F = e^{-\tau}$, where τ is the Lyα optical depth

$$\tau_\alpha(i) = \frac{c\sigma_\alpha \delta R}{\pi^{1/2}} \sum_{j=1}^{N} \frac{n_{\mathrm{HI}}}{b_{\mathrm{HI}}(j)} \exp\left[-\left(\frac{v_{\mathrm{H}}(i) - u(j)}{b_{\mathrm{HI}}(j)} \right)^2 \right]. \quad (11)$$

Here i and j denote pixels along the line of sight through the simulation volume, δR is the (proper) pixel width, $\sigma_\alpha = 4.48 \times 10^{-18}$ cm^2 is the scattering cross-section for Lyα photons, $b_{\mathrm{HI}} = (\frac{2k_{\mathrm{B}}T}{m_{\mathrm{H}}})^{1/2}$ is the Doppler parameter describing the thermal width of the line

profiles, $v_{\rm H}$ is the Hubble velocity and $u(j)$ is the total velocity given by the summation of the Hubble flow and the peculiar velocity along the line of sight, $u(j) = v_{\rm H}(j) + v_{\rm pec}(j)$. After constructing our synthetic Lyα forest spectra, we renormalize the pixel optical depths to match the mean observed Lyα flux at $z = 2.5$ from the high-resolution sample of Faucher-Giguère et al. (2008).

4.1 Synthetic Lyα forest spectra

In Fig. 3, we display a synthetic Lyα forest spectrum drawn through our 1 Gpc^3 simulation volume. In the first panel, we show the line-of-sight IGM density contrast while in the second we show the average excess energy per He II photoionization. This particular line of sight passes nearby several quasars, with their locations corresponding to the minima where $\langle E_{\rm He\,II}\rangle \sim 20\,{\rm eV}$. These

minima arise due to heating close to the quasars being dominated by ionizing photons near the He II ionization edge which have shorter mean free paths. Additionally, $\langle E_{\rm He\,II}\rangle \sim 50$–$60\,{\rm eV}$ furthest from the quasars, is only a factor of 2 lower than the theoretical maximum value expected if every ionizing photon were absorbed with equal probability, such that $\langle E\rangle_{\rm thick} = h_{\rm p}\nu_{\rm He\,II}/(\alpha_{\rm s} - 1) = 108.8\,{\rm eV}$ (Abel & Haehnelt 1999).

In the third and fourth panels of Fig. 3, we compare the H I fraction ($X_{\rm H\,I} = n_{\rm H\,I}/n_{\rm H}$) and IGM temperature in our two scenarios. The red curves correspond to the model without temperature fluctuations. We observe that the IGM temperature fluctuations have an important impact on the H I fraction through the temperature dependence of the H II recombination coefficient, $\alpha_{\rm H\,I} \propto T^{-0.7}$. The largest difference between the models occurs in the regions where the mean excess energy per photoionization is greatest, resulting in a decrease in
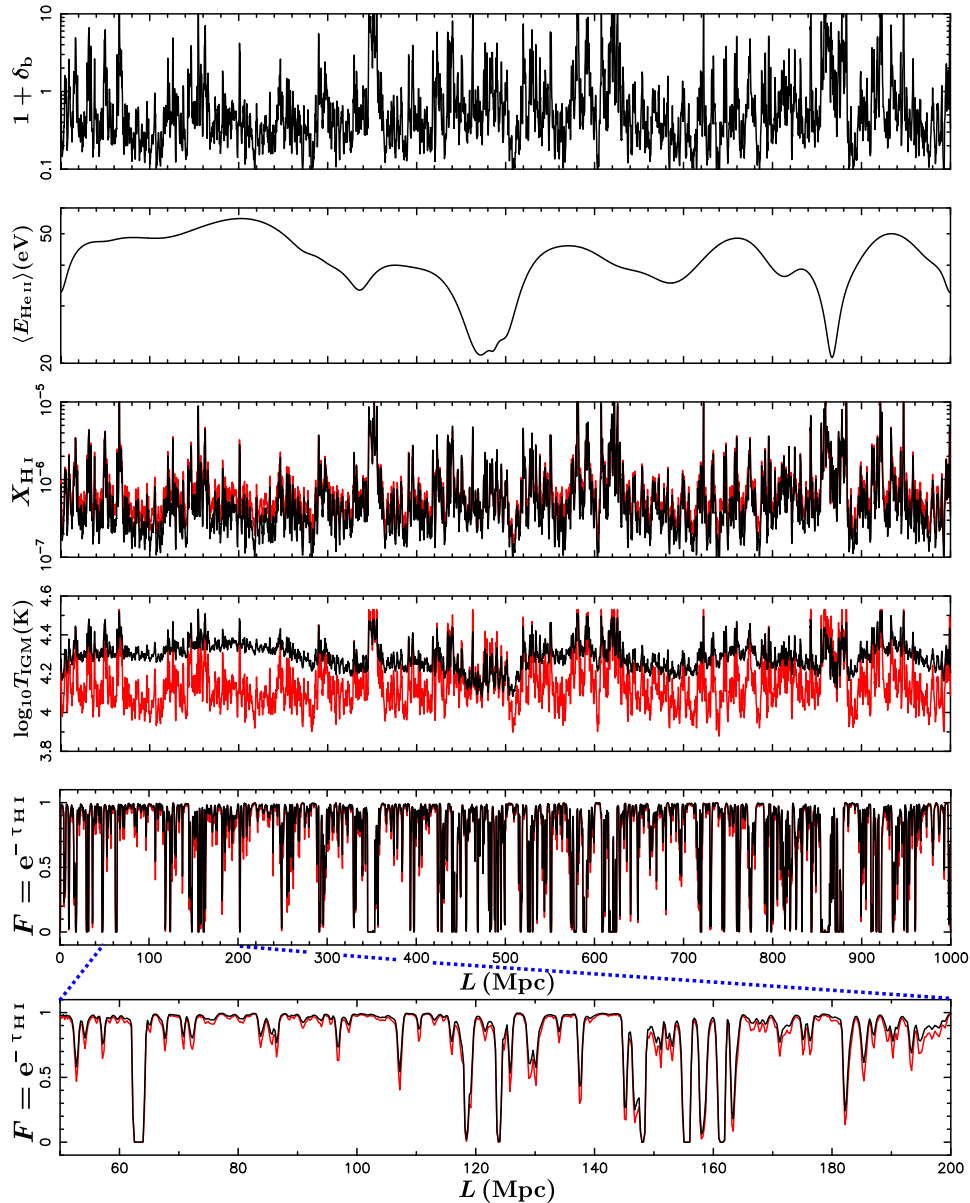

Figure 3. A line of sight drawn randomly through our Lyα forest simulation. From top to bottom, the panels display: the rank-ordered IGM density contrast; the average excess energy per He II ionization; the H I fraction $X_{\rm H\,I} = n_{\rm H\,I}/n_{\rm H}$; the gas temperature; the transmitted fraction $F = e^{-\tau}$, and a 150 Mpc zoom in of the Lyα forest spectrum in the previous panel. In all panels, the black (red) curves display models including (excluding) the large-scale temperature fluctuations computed using equation (8).

the H I fraction by as much as 60 per cent. As noted earlier, the IGM temperature in our model with patchy He II photoheating is on average systematically higher compared to a single temperature–density power-law relation. Large-scale (greater than a few hundred Mpc) variations result in the gas temperature, and are driven by the heating from long range, hard ionizing photons.

The final two panels in Fig. 3 provide a direct comparison of the transmitted fraction in the Lyα forest. Note that for the purpose of this comparison only we have not normalized the spectra to the same effective optical depth. As expected there is less transmission overall from the model without temperature fluctuations, although the differences are small and are only apparent on large scales. As noted by McQuinn et al. (2011), it is for this reason that detecting $\Delta T \sim 10^4$ K temperature fluctuations from He II reionization is difficult using 1D line-of-sight Lyα forest statistics based on a handful of quasar spectra (see also Theuns et al. 2002; Lai et al. 2006; Lidz et al. 2010). While we do not explicitly show here the impact of the IGM temperature fluctuations on the 1D Lyα flux power spectrum and probability distribution function, we find that the level of variation between the models is small, and is at most of the order of 5 per cent. Note, however, Lee & Spergel (2011) suggest an analysis of the 1D Lyα transmission with threshold probability functions may yield additional sensitivity to these large IGM temperature fluctuations.

4.2 The 3D Lyα forest power spectrum

Large-scale temperature fluctuations are expected to have a small effect on individual Lyα forest spectra and on 1D line-of-sight statistics. However, in the case of the three-dimensional clustering measurements from the Lyα forest, temperature fluctuations may be much more important (see also White et al. 2010; McQuinn et al. 2011). We thus estimate the impact of the temperature fluctuations on the large-scale clustering measurements of the Lyα forest by taking the ratio of the spherically averaged 3D Lyα forest power spectrum from our simulations with patchy He II photoheating and a model without temperature fluctuations. Our reconstruction of the un-aliased estimate of the 3D Lyα forest spectrum (which arises

due to the sparsely sampled Lyα forest number density) follows the method outlined by McDonald & Eisenstein (2007) as applied in GBW11.

In this work, we assess our Lyα forest modelling in the context of the recent BOSS observations. We therefore process our synthetic spectra to mimic the BOSS instrumental resolution by convolving the data with a Gaussian with an FWHM of ∼3.63 Å followed by a resampling on to bins of width ∼1.04 Å. We also use the nominal mean survey design parameters of BOSS, where we measure our 3D Lyα forest power spectrum with a quasar density of 15 deg^{-2} and add S/N = 5 per pixel (Bolton et al. 2012; Dawson et al. 2013). Note also we only consider line-of-sight sections of the forest corresponding to the distance between the rest frame Lyα and Lyβ transitions at $z = 2.5$ (roughly ∼620 Mpc). For each of the 10 realizations we performed, we then generate 60 000 lines of sight within each simulation box and randomly sample each at our prescribed line-of-sight density to recover the 3D Lyα forest power spectrum 100 times. In this manner, we gain a good estimate of the impact of large-scale temperature fluctuations within each simulation volume.

In the left-hand panel of Fig. 4, we show the median spherically averaged 3D Lyα forest power spectrum computed from our two scenarios. Here, the model with patchy He II photoheating is represented by the solid curve, while the model without temperature fluctuations is given by the dashed curve. Note again that to construct these data, we recover the median power spectrum across all of our 10 realizations. Therefore, these represent the median across a sample of 1000 individual power spectra. An increase in power on scales $k < 0.1$ Mpc^{-1} is evident in the model with patchy heating. The error bars show the 1σ Poisson errors for a single estimate of the spherically averaged 3D Lyα forest power spectrum. At $k < 0.02$ Mpc^{-1}, the limited number of k-space bins sampled at these large scales results in significant Poisson scatter which exceeds the difference between the two models (our box size corresponds to $k = 6.2 \times 10^{-3}$ Mpc^{-1}, and the path length between Lyα and Lyβ is $k \sim 0.01$ Mpc^{-1}). Our results for the 3D power spectrum at $k < 0.02$ Mpc^{-1} should therefore be interpreted with caution.
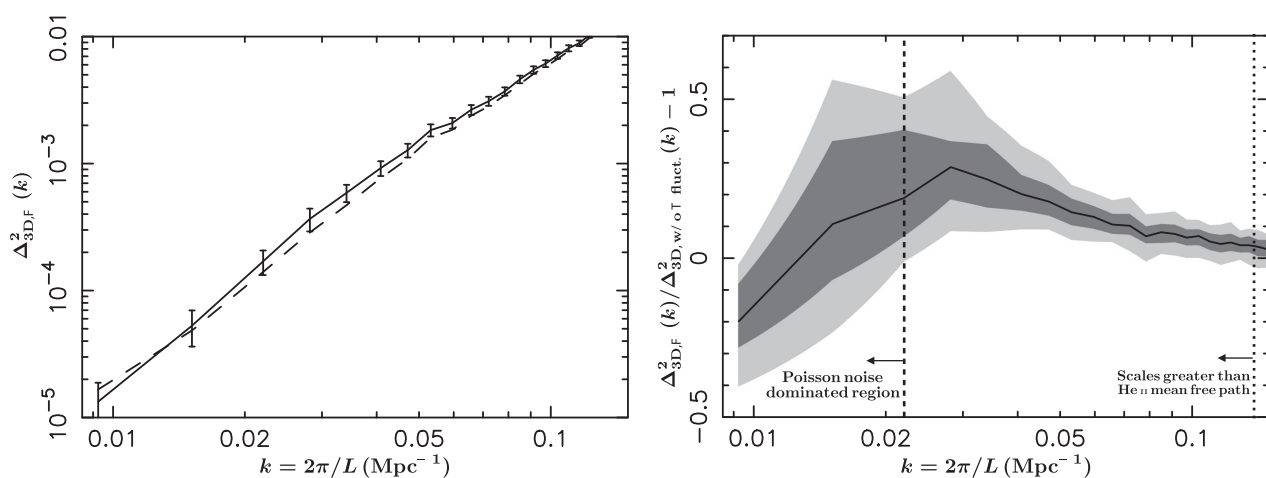

Figure 4. The reconstructed spherically averaged dimensionless 3D Lyα forest power spectrum obtained from our simulations. Left-hand panel: the median power spectrum from our patchy He II photoheating model (solid curve) and our model without IGM temperature fluctuations (dashed curve). The error bars give the 1σ Poisson errors on the number of Fourier modes within each spherical shell in k-space. Right-hand panel: the median fractional variation in the 3D power spectra obtained from our simulations. The shaded regions correspond to the predicted 68 and 95 per cent scatter around the median. Wavenumbers less than the vertical dashed line correspond to a Poisson noise dominated regime at scales approaching the box size, while wavenumbers left of the vertical dotted line denote scales greater than the mean free path at the He II ionization edge ($\lambda_{\mathrm{He\,II}} = 45$ Mpc) assumed in our model.

Keeping this in mind, in the right-hand panel of Fig. 4, we show the fractional variation in the median spherically averaged 3D Lyα forest power spectrum relative to the model excluding large-scale temperature fluctuations. The shaded regions correspond to the 68 and 95 per cent scatter (dark and light grey, respectively) around the median fractional variance. Furthermore, the dotted line represents the wavenumber corresponding to the He II mean free path at 4 Ryd assumed in our model ($\lambda_{\mathrm{He\,II}} = 45\,\mathrm{Mpc}$). Importantly, it is only on spatial scales significantly larger than the mean free path at the ionization edge where the temperature fluctuations have a notable impact on the large-scale power. This is in part because it is the long range heating by hard photons which are responsible for producing the largest temperature (and hence H I fraction) fluctuations in our model. At spatial scales corresponding to $k \sim 0.02\,\mathrm{Mpc}^{-1}$, the temperature fluctuations increase large-scale power up to 20–30 per cent, with the 95 per cent scatter around the median showing an increase of up to $\sim$60 per cent. Furthermore, this is a scale-dependent effect. At decreasing spatial scales (larger k), the amplitude of the temperature fluctuations is smaller, and the temperature fluctuations have a limited effect on the power spectrum at $k > 0.1\,\mathrm{Mpc}^{-1}$. Note, however, that this inference is model dependent. In particular, if the mean free path for He II ionizing photons is larger than we have assumed, or if the sources responsible for reionizing He II are more numerous and/or less clustered, we expect the effect of temperature fluctuations on the large-scale power to be smaller. Our results nevertheless suggest that with detailed forward modelling of the 3D Lyα forest power spectrum, it may be possible to probe the inhomogeneous thermal state of the IGM following He II reionization with existing and forthcoming spectroscopic surveys.

In previous work, Pontzen (2014) and Gontcho A Gontcho et al. (2014) constructed analytical models that serve to illustrate the dominant contributions to variations in the H I clustering power. However, both studies focus on spatial fluctuations in the ionizing background, which as discussed earlier will operate on somewhat larger scales than the temperature fluctuations considered here. Gontcho A Gontcho et al. (2014) do briefly address the potential effect of photoheating during He II reionization, finding a rather small impact on the Lyα correlation function. However, these authors use the intensity of the He II ionizing radiation (rather than the mean excess energy per He II ionization) to compute the bias factor for thermal fluctuations in their model. This may not fully capture the important effect hard photons with long mean free paths have on the photoheating rate. On the other hand, using a combination of numerical and analytical modelling McQuinn et al. (2011) observe that temperature fluctuations increase large-scale power by order unity on scales $k < 0.1\,\mathrm{Mpc}^{-1}$, again suggesting that our semi-analytical model captures the effect of the temperature fluctuations reasonably well.

It is also worth noting that none of these models include the effect of winds on the IGM. Recently, Viel, Schaye & Booth (2013) have shown that AGN and supernova-driven winds can impact on 1D Lyα forest flux statistics. While the magnitude of the effect is not large, the statistical power of the BOSS data will render these effects non-negligible. How winds would impact upon the 3D Lyα forest power spectrum on large scales, however, remains uncertain, although these effects are most prominent in the small-scale modes of the line-of-sight Lyα forest power spectrum, and should occur on spatial scales smaller than the IGM temperature fluctuations considered here.

Finally, it is important to note that although we have only considered the 3D Lyα forest power spectrum, astrophysical information may also be drawn from cross-correlations of the Lyα forest with either DLAs (Font-Ribera et al. 2012b) or quasars (Font-Ribera et al. 2013). Large-scale IGM temperature fluctuations could imprint a signature on to the quasar–Lyα forest cross-correlation which is now measured to 80 h^{-1} Mpc (Font-Ribera et al. 2013), although disentangling this signature from the quasar clustering and ionization fluctuations may be challenging.

4.3 Recovery of the BAO scale

We now briefly turn our attention to the impact of large-scale IGM temperature fluctuations on the recovery of the BAO scale. A number of studies have already noted that fluctuations in the ionizing background may add broad-band power to the 3D Lyα forest correlation function, which could be fitted and marginalized over by the addition of a smoothed component (Slosar et al. 2009; McQuinn et al. 2011; Gontcho A Gontcho et al. 2014; Pontzen 2014). In the case of strong ionizing background fluctuations, both Slosar et al. (2009) and Pontzen (2014) observed that these could shift the recovered BAO position by a few per cent, although this is within the noise of the BAO measurements from BOSS (Busca et al. 2013; Slosar et al. 2013; Delubac et al. 2014; Font-Ribera et al. 2014).

Consequently, to similarly assess the impact of temperature fluctuations on the recovery of the BAO scale, we closely follow the approach used in GBW11. We perform two concurrent Lyα forest simulations, one with and one without BAOs. We then take the ratio of the 3D Lyα forest power spectra predicted by these two simulations, and recover an estimate of the BAO scale using a simple two parameter model. We perform this test for models including and excluding patchy He II photoheating. In both cases, we confirm there is little impact on the recovery of the BAO scale. The large-scale temperature fluctuations result only in the addition of a smooth, scale-dependent increase in power that can potentially be marginalized over. Nevertheless, as the *significance* of the recovered BAO peak is often inferred relative to the null hypothesis of no BAO peak, this broad-band term is important. Consequently, a complete forward modelling of the broad-band term in the Lyα correlation function will require the incorporation of both ionizing background and temperature fluctuations.

5 CONCLUSIONS

The recovery of the large-scale clustering of the IGM and the BAO feature from the Lyα forest measured by BOSS (Busca et al. 2013; Slosar et al. 2013; Delubac et al. 2014; Font-Ribera et al. 2014) provide a new avenue for precision cosmology from the Lyα forest at high-z. In addition, the wealth of observational data also provides a unique opportunity to explore the thermal state of the IGM following the epoch of He II reionization. However, the impact of patchy He II photoheating on the IGM is subtle, requiring detailed modelling to extract its signature from large spectroscopic data sets.

In this work, we have therefore developed a semi-analytical model for investigating the impact of large-scale temperature fluctuations on the three-dimensional clustering of the Lyα forest. Our method is built upon an existing efficient, large-volume, mock Lyα forest survey model developed by Greig et al. (2011). We have modified this model to include several key ingredients required for modelling the IGM following He II reionization, including quasar clustering, a spatially varying ionizing background and inhomogeneous He II photoheating.

We find our simple prescription for patchy He II photoheating is in very good agreement with the results from recent RT simulations of He II reionization (McQuinn et al. 2009; Compostella et al. 2013).

However, the dynamic range of our modelling is substantially larger than currently possible with these more expensive, fully numerical approaches. Large-scale temperature fluctuations typically produce a 20–30 per cent increase in the 3D spherically averaged Lyα forest power spectrum at $k \sim 0.02\,\mathrm{Mpc}^{-1}$, although scatter arising from cosmic variance indicates this can be as large as 50–60 per cent. Importantly, we also observe this to be a scale-dependent effect with an amplitude that increases towards larger spatial scales. Furthermore, this effect is expected to occur at scales larger than both the mean quasar separation and the mean free path of He II ionizing photons at the photoelectric edge. We note, however, that our results are model dependent. An increase in the mean free path for He II ionizing photons, or more numerous or less clustered ionizing sources will result in a reduction in the increase of large-scale power. Nevertheless, with detailed forward modelling, it may be possible to probe the inhomogeneous thermal state of the IGM following He II reionization with existing and forthcoming spectroscopic surveys.

Finally, we briefly consider the potential systematic uncertainty that large-scale temperature fluctuations may have on the recovery of the BAO scale. We find that these do not substantially impact upon the recovery of the BAO scale; large-scale temperature fluctuations result only in the addition of smooth, scale-dependent increase in power that can potentially be marginalized over. However, any complete forward modelling of the broad-band term in the Lyα correlation function will ultimately require the incorporation of both ionizing background (Slosar et al. 2009; White et al. 2010; Gontcho A Gontcho et al. 2014; Pontzen 2014) *and* large-scale thermal fluctuations.

ACKNOWLEDGEMENTS

REFERENCES

Abel T., Haehnelt M. G., 1999, ApJ, 520, L13
Becker G. D., Bolton J. S., Haehnelt M. G., Sargent W. L. W., 2011, MNRAS, 410, 1096
Bolton J. S., Viel M., 2011, MNRAS, 414, 241
Bolton J. S., Oh S. P., Furlanetto S. R., 2009, MNRAS, 395, 736
Bolton J. S., Becker G. D., Wyithe J. S. B., Haehnelt M. G., Sargent W. L. W., 2010, MNRAS, 406, 612
Bolton A. S. et al., 2012, AJ, 144, 144
Busca N. G. et al., 2013, A&A, 552, 96
Compostella M., Cantalupo S., Porciani C., 2013, MNRAS, 435, 3169
Croft R. A. C., Weinberg D. H., Katz N., Hernquist L., 1998, ApJ, 495, 44
Croft R. A. C., Weinberg D. H., Bolte M., Burles S., Hernquist L., Katz N., Kirkman D., Tytler D., 2002, ApJ, 581, 20
Davies F. B., Furlanetto S. R., 2014, MNRAS, 437, 1141
Dawson K. S. et al., 2013, AJ, 145, 10
Delubac T. et al., 2014, preprint (arXiv:1404.1801)
Fardal M. A., Giroux M. L., Shull J. M., 1998, AJ, 115, 2206
Faucher-Giguère C.-A., Prochaska J. X., Lidz A., Hernquist L., Zaldarriaga M., 2008, ApJ, 681, 831
Font-Ribera A., McDonald P., Miralda-Escudé J., 2012a, J. Cosmol. Astropart. Phys., 01, 001
Font-Ribera A. et al., 2012b, J. Cosmol. Astropart. Phys., 11, 059
Font-Ribera A. et al., 2013, J. Cosmol. Astropart. Phys., 05, 018
Font-Ribera A. et al., 2014, J. Cosmol. Astropart. Phys., 5, 27
Furlanetto S. R., 2009, ApJ, 703, 702
Furlanetto S. R., Oh S. P., 2008a, ApJ, 681, 1
Furlanetto S. R., Oh S. P., 2008b, ApJ, 682, 14
Gontcho A Gontcho S., Miralda-Escudé J., Busca N. G., 2014, MNRAS, 442, 187
Greig B., Bolton J. S., Wyithe J. S. B., 2011, MNRAS, 418, 1980 (GBW11)
Haardt F., Madau P., 2012, ApJ, 746, 125
Hopkins P. F., Richards G. T., Hernquist L., 2007, ApJ, 654, 731
Hui L., Gnedin N. Y., 1997, MNRAS, 292, 27
Khaire V., Srianand R., 2013, MNRAS, 431, L53
Lai K., Lidz A., Hernquist L., Zaldarriaga M., 2006, ApJ, 644, 61
Le Goff J. M. et al., 2011, A&A, 534, A135
Lee K.-G., Spergel D. N., 2011, ApJ, 734, 21
Lidz A., Malloy M., 2014, ApJ, 788, 175
Lidz A., Faucher-Giguère C.-A., Dall'Aglio A., McQuinn M., Fechner C., Zaldarriaga M., Hernquist L., Dutta S., 2010, ApJ, 718, 199
Lukić Z., Stark C., Nugent P., White M., Meiksin A., Almgren A., 2015, MNRAS, 446, 3697
McDonald P., Eisenstein D. J., 2007, Phys. Rev. D, 76, 063009
McDonald P. et al., 2006, ApJS, 163, 80
McQuinn M., Lidz A., Zaldarriaga M., Hernquist L., Hopkins P. F., Dutta S., Faucher-Giguère C.-A., 2009, ApJ, 694, 842
McQuinn M., Hernquist L., Lidz A., Zaldarriaga M., 2011, MNRAS, 415, 977
Madau P., Haardt F., Rees M. J., 1999, ApJ, 514, 648
Meiksin A., Tittley E. R., 2012, MNRAS, 423, 7
O'Meara J. M., Prochaska J. X., Worseck G., Chen H.-W., Madau P., 2013, ApJ, 765, 137
Palanque-Delabrouille N. et al., 2013, A&A, 559, A85
Peirani S., Weinberg D. H., Colombi S., Blaizot J., Dubois Y., Pichon C., 2014, ApJ, 784, 11
Planck Collaboration XVI, 2014, A&A, 571, A16
Pontzen A., 2014, Phys. Rev. D, 89, 083010
Raskutti S., Bolton J. S., Wyithe J. S. B., Becker G. D., 2012, MNRAS, 421, 1969
Rauch M., 1998, ARA&A, 36, 267
Rudie G. C., Steidel C. C., Shapley A. E., Pettini M., 2013, ApJ, 769, 146
Schaye J., Theuns T., Rauch M., Efstathiou G., Sargent W. L. W., 2000, MNRAS, 318, 817
Seljak U., Slosar A., McDonald P., 2006, J. Cosmol. Astropart. Phys., 10, 014
Shen Y. et al., 2007, AJ, 133, 2222
Shull J. M., van Steenberg M. E., 1985, ApJ, 298, 268
Shull J. M., Stevans M., Danforth C. W., 2012, ApJ, 752, 162
Slosar A., Ho S., White M., Louis T., 2009, J. Cosmol. Astropart. Phys., 10, 019
Slosar A. et al., 2013, J. Cosmol. Astropart. Phys., 04, 026
Stevans M. L., Shull J. M., Danforth C. W., Tilton E. M., 2014, ApJ, 794, 75
Telfer R. C., Zheng W., Kriss G. A., Davidsen A. F., 2002, ApJ, 565, 773
Theuns T., Leonard A., Efstathiou G., Pearce F. R., Thomas P. A., 1998, MNRAS, 301, 478
Theuns T., Zaroubi S., Kim T.-S., Tzanavaris P., Carswell R. F., 2002, MNRAS, 332, 367
Viel M., Matarrese S., Mo H. J., Theuns T., Haehnelt M. G., 2002, MNRAS, 336, 685
Viel M., Haehnelt M. G., Springel V., 2004, MNRAS, 354, 684
Viel M., Schaye J., Booth C. M., 2013, MNRAS, 429, 1734
White M., Pope A., Carlson J., Heitmann K., Habib S., Fasel P., Daniel D., Lukic Z., 2010, ApJ, 713, 383

This paper has been typeset from a TEX/LATEX file prepared by the author.